Dentomaxillofacial Radiology (2013) 42, 92555893

http://dmfr.birjournals.org

RESEARCH

Dosimetry of a cone beam CT device for oral and maxillofacial radiology using Monte Carlo techniques and ICRP adult reference computational phantoms

JJ Morant*[,1], M Salvadó[2], I Hernández-Girón[2,3], R Casanovas[2], R Ortega[4] and A Calzado[3]

[1]*Universitat Rovira i Virgili, Servei de Protecció Radiolgòica, Reus, Spain;* [2]*Universitat Rovira i Virgili, Física Mèdica, Reus, Spain;* [3]*Universidad Complutense de Madrid, Departamento de Radiología, Madrid, Spain;* [4]*Universidad Complutense de Madrid, Departamento de Estomatología III, Madrid, Spain*

Objectives: The aim of this study was to calculate organ and effective doses for a range of available protocols in a particular cone beam CT (CBCT) scanner dedicated to dentistry and to derive effective dose conversion factors.
Methods: Monte Carlo simulations were used to calculate organ and effective doses using the International Commission on Radiological Protection voxel adult male and female reference phantoms (AM and AF) in an i-CAT CBCT. Nine different fields of view (FOVs) were simulated considering full- and half-rotation modes, and also a high-resolution acquisition for a particular protocol. Dose–area product (DAP) was measured.
Results: Dose to organs varied for the different FOVs, usually being higher in the AF phantom. For 360°, effective doses were in the range of 25–66 μSv, and 46 μSv for full head. Higher contributions to the effective dose corresponded to the remainder (31%; 27–36 range), salivary glands (23%; 20–29%), thyroid (13%; 8–17%), red bone marrow (10%; 9–11%) and oesophagus (7%; 4–10%). The high-resolution protocol doubled the standard resolution doses. DAP values were between 181 mGy cm^2 and 556 mGy cm^2 for 360°. For 180° protocols, dose to organs, effective dose and DAP were approximately 40% lower. A conversion factor (DAP to effective dose) of 0.130 ± 0.006 μSv mGy^{-1} cm^{-2} was derived for all the protocols, excluding full head. A wide variation in dose to eye lens and thyroid was found when shifting the FOV in the AF phantom.
Conclusions: Organ and effective doses varied according to field size, acquisition angle and positioning of the beam relative to radiosensitive organs. Good positive correlation between calculated effective dose and measured DAP was found.
Dentomaxillofacial Radiology (2013) **42,** 92555893. doi: 10.1259/dmfr/92555893

Cite this article as: Morant JJ, Salvadó M, Hernández-Girón I, Casanovas R, Ortega R, Calzado A. Dosimetry of a cone beam CT device for oral and maxillofacial radiology using Monte Carlo techniques and ICRP adult reference computational phantoms. *Dentomaxillofac Radiol* 2013; **42:** 92555893.

Keywords: dental equipment; Monte Carlo method; cone beam CT; radiation dosimetry; radiological phantoms

Introduction

Cone beam CT (CBCT) scanners are increasingly being used in many dental specialties, such as orthodontics, implantology, trauma and dental surgery. Compared with conventional CT, they offer several advantages, especially a significant reduction in the imparted patient doses.[1,2] These devices produce both two-dimensional and three-dimensional images that are adapted to the clinical requirements for a correct diagnosis and treatment planning. These facts have fostered the recent growth in the number of manufacturers and models of

*Correspondence to: Mr Juan-Jose Morant, Universitat Rovira i Virgili. Servei de Protecci Radiològica Sant Llorenç 21, 43201 Reus, Spain. E-mail: juanjose.morant@urv.cat
Received 18 April 2012; revised 14 June 2012; accepted 30 June 2012

CBCT.[3,4] Most of these devices have a standard protocol available with acquisition parameters and voxel sizes that are appropriate for the average patient. Additionally, the user can select from a range of protocols the most suitable to the clinical requirements and anatomical characteristics of the patient. Because the radiation dose received by the patient depends primarily on the field of view (FOV) and the selected exposure parameters, it is important to choose the protocol that imparts the lowest patient dose while providing the required diagnostic information.[5]

The latest recommendations from the International Commission on Radiological Protection (ICRP) have modified the values of the weighting factors of several organs for the calculation of the effective dose and have added new organs or tissues to those previously included in the 1990 recommendations.[6,7] The most significant change for dental radiological examinations is the inclusion of salivary glands as an individually weighted tissue and of the oral mucosa into the remainder organs. Additionally, the weighting factor for the remainder has increased from 0.05 to 0.12 so that other organs in this category, which are usually in the primary beam on CBCT scans (extrathoracic region and lymphatic nodules), have also increased their contribution to the effective dose. A number of studies have assessed the influence of these changes on the effective dose of patients undergoing CBCT examinations of the oral and maxillofacial region.[8–11]

To date, published dosimetric studies reflect a wide patient dose range to reach similar diagnostic tasks; however, the effective dose from CBCT examinations is several to many times greater than conventional panoramic imaging and lower by more than an order of magnitude than reported doses for conventional CT.[12–14] Most of these values are derived from measurements using thermoluminescence dosemeters (TLDs) that are placed within anthropomorphic phantoms to assess typical patient doses.[1,2,9–14] For the physical phantoms used in these studies, the position and size of radiosensitive organs have been estimated. This method, although providing organ doses and effective dose values compatible with commonly accepted uncertainties in the assessment of these quantities, has a number of drawbacks. Several of these drawbacks arise from the use of a limited number of TLDs for assessing doses in large organs or tissues, unless an adequate number of TLDs is used to minimize the variability of organ dose calculations.[14] Moreover, the TLD chip positioning can also be critical when a fraction of an organ is irradiated during the scan or for organs in the neighbourhood of the scanned region. All of these limitations can be substantially reduced by using Monte Carlo (MC) simulations combined with organ dose calculations within anatomically realistic anthropomorphic phantoms.

In a previous study, an MC simulation program was developed and validated to be applied to a CBCT device to calculate the radiation dose in voxel objects.[15] ICRP have published voxel-based phantoms for male (AM) and female (AF) adults. These phantoms are reference computational models based on computed tomographic data of real adult people and, hence, are digital three-dimensional representations of human anatomy.[16] To our knowledge, there are few reports that have focused on the radiation dose of CBCT using MC techniques.[17] Moreover, there are no reports using the ICRP AM/AF phantoms for this task. The aim of this study was to calculate organ doses and effective doses to a typical patient for a range of available protocols in a particular CBCT scanner that is dedicated to dental radiology. For this task, the ICRP AM/AF phantoms were implemented in our MC simulation program. Additionally, a secondary objective of the work was to derive conversion factors to estimate the effective dose for the protocols analysed.

Materials and methods

Cone beam CT device

This work was performed using a next-generation i-CAT dental CBCT scanner (Imaging Sciences International, Hatfield, PA) that consisted of an X-ray tube with a stationary anode and a $20 \times 25 cm^2$ amorphous silicon flat panel detector with a CsI scintillator.

A bow-tie filter placed in the X-ray beam path provides size-adapted compensation for the variation of head thickness from the centre to the periphery of the field. The user can select up to nine possible default radiation fields to fit to the anatomical characteristics of the patient and the volume under study by collimation. The pulsed X-ray emission is controlled by a high-frequency generator. The X-ray tube operates at 120 kVp and 5 mA, which are both fixed; rotation time can be selected between 8.9 s and 26.9 s for 360° (full rotation) acquisitions or between 4.8 s and 14.7 s for 180° (half rotation). The images can be reconstructed in five different voxel sizes: 0.4 mm, 0.3 mm, 0.25 mm, 0.2 mm or 0.125 mm. The available options vary according to the selected protocol.

ICRP AM/AF phantoms

The reference computational models for male (AM) and female (AF) proposed by ICRP were used in the study.[16] These phantoms were constructed from CT images of real patients, and the mass, spatial distribution and composition of each organ and tissue were adapted to match the ICRP standards for adult men (AM) and women (AF) without compromising their anatomical

Table 1 Primary International Commission on Radiological Protection voxel phantom characteristics. The height and mass reference values are in parentheses

Characteristic	*AM phantom*	*AF phantom*
Gender	Male	Female
Age	38 y	43 y
Height (reference) (cm)	176 (176)	167 (163)
Mass (reference) (kg)	<70 (73)	59 (60)
Number of voxels per slab	254 × 127	299 × 137
Number of slabs	222	348
Voxel size (mm^3)	2.137 × 2.137 × 8	1.775 × 1.775 × 4.84

AF, adult female; AM, adult male.

realism. A summary of the anatomical features and data related to the phantoms is shown in Table1.

The implementation of AM and AF phantoms in the simulation program required localization of all organs and tissues within them and an assignment of their composition as provided in the ICRP report. Accordingly, details concerning the 141 organs or tissues and 53 materials (*i.e.* chemical composition and density) were included for each phantom. Both phantoms contain an additional subsegmentation for the skeleton which was also implemented in the MC program. This subsegmentation is needed because bone spongiosa has a microscopic structure that cannot be correctly represented in the volume of each voxel. Consequently, 44 categories of skeletal tissue composed of 20 different materials according to their content of red bone marrow (RBM), yellow bone marrow (YBM) and endosteum were implemented for both phantoms. Each voxel is considered homogeneously composed of 1 of these 20 materials with a specific mass fraction of RBM, YBM and endosteum. For the calculation of the effective dose, the required 27 organs/tissues were identified in each phantom.

To validate the correct implementation of all the related information in the MC program, the total mass of every organ and material in the model were computed and the results were compared with the original data.

Protocols

Nine different cylindrical scan volumes predefined (diameter × height) by the device were selected: (a) Ø16 × 13 cm height; (b) Ø16 × 11 cm height; (c) Ø16 × 10 cm height; (d) Ø16 × 8 cm height; (e) Ø16 × 6 cm height (maxilla); (f) Ø16 × 6 cm height (mandible); (g) Ø8 × 8 cm height; (h) Ø16 × 4 cm height; and (i) full head Ø23 × 17 cm height. All protocols were simulated for a standard resolution (0.3–0.4 mm voxel) and both 360° (18.54 mAs) and 180° (10.11 mAs) acquisition modes. It is important to notice that during half-rotation acquisitions, the X-ray tube rotates behind the patient's head, which can influence the dose distribution.

To test the dependence of dose with tube loading settings, a high resolution (*i.e.* Ø16 × 13 cm height) protocol was also simulated for 360° (37.07 mAs) and 180° (20.27 mAs) acquisitions. The organ/tissue doses were calculated separately for the AF and AM phantoms in each case.

Additionally, the effect of varying the isocentre along the *z*-axis on the eye lens and thyroid doses was investigated using the standard protocol (Ø16 × 13 cm) on the AF phantom. To accomplish this, different FOV positions within the dentomaxillofacial region were simulated by shifting the isocentre along the *z*-axis at constant intervals of either 2 mm, to calculate the dose to the eye lens, or 10 mm for thyroid dose calculation. Owing to its morphological characteristics, the ICRP AF phantom is more sensitive to dose variations with FOV position, and hence it was selected for this task. The reason for this is that the thyroid in the ICRP AF phantom is closer to the occlusal plane and its size along the *z*-axis is smaller, which makes it more likely to be partially or fully inside the direct beam.

Monte Carlo simulation

The developed MC program simulates the radiation transport through the voxelized space. A benchmarked Electron Gamma Shower V4 (EGS4) package in combination with the low-energy photon-scattering expansion (National Laboratory for High Energy Physics (KEK), Tsukuba, Japan) are the basis for radiation transport. Cut-off energies of 5 keV and 30 keV were used for photons and electrons, respectively, in this study.[18,19]

All of the parameters that influence doses were considered in the simulation. The spectral and geometric characteristics of the X-ray beam (*i.e.* peak tube potential, primary filtration, bow-tie filter attenuation, and heel and penumbra effects caused by the focus and collimator) were modelled. Additionally, the values of other protocol-specific acquisition parameters, such as starting and ending exposure angles for 360° or 180° rotation, tube loading, overlapping beam angle, frequency of radiation pulses and field size, were used as inputs.[15] The FOV of the investigated CBCT is a cylindrical volume generated by rotation of the beam cross-section at the isocentre. The FOV height was implemented as the sum of the distances from the upper and lower cylinder surfaces to the occlusal plane. The FOV diameter was implemented directly for all the protocols under study, except for the full head Ø23 × 17 cm height. For full head height, as the centre of rotation does not coincide with the centre of radiation, the FOV diameter was taken as twice the distance from the cylinder lateral surface to the rotational axis. Therefore, the significant field asymmetry in many protocols, noticeable in the full head Ø23 × 17 cm height, was modelled.

As an example of field implementation, Figure 1 shows the Ø16 × 13 cm FOV superimposed on the middle sagittal plane of each ICRP phantom. It is noteworthy that the positioning of the isocentre in the two phantoms can be different from clinical situations. In the adult female (left-hand image), the radiation field should be collimated to avoid some organs, such as thyroid, eye lenses or salivary glands, being included in the primary beam and lowering the dose imparted to them.

The whole anatomy of the ICRP AM phantom (*i.e.* 222 slabs of 8 mm thickness, Table 1) was used as an EGS4 input file. By contrast, the ICRP AF phantom, which consists of 348 slabs of 4 mm thickness (Table 1) was truncated for the simulation. The slabs making up the lower limbs of this phantom were excluded to meet the EGS4 input file size requirements (252 slabs maximum). This fact has no impact on the results because, on the one hand, the energy imparted to the legs in a dental CBCT examination is negligible, and, on the other hand, the total mass of the leg tissues was considered for organ dose calculation.

The MC simulations were performed in a cluster that comprised 14 Bull Nova Scale R422E1 servers (Bull SAS, Les Clayes-sous-Bois, France) with 28 nodes and

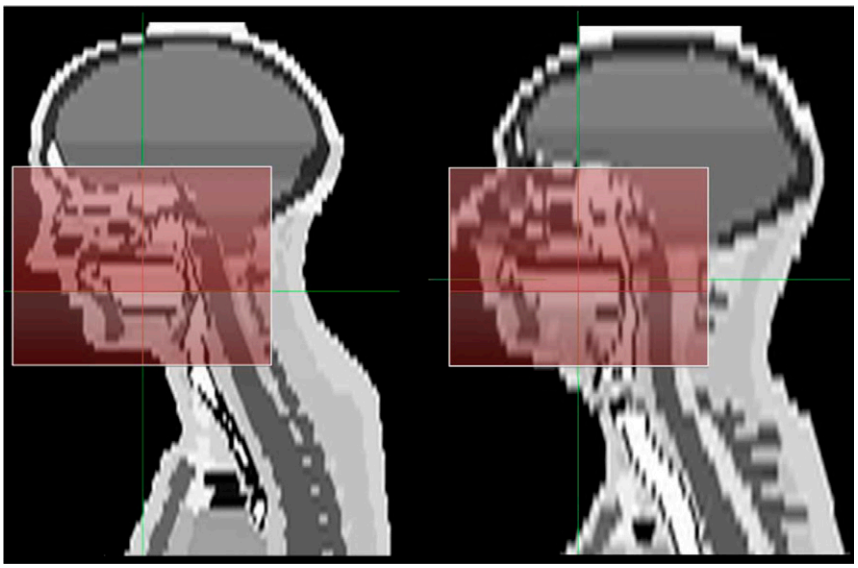

Figure 1 A middle sagittal section of the International Commission on Radiological Protection adult female (left) and adult male (right) phantoms. The overlaid rectangles represent the radiation field borders for a Ø16 × 13 cm height acquisition

56 Xeon 4 core processors (Intel, Santa Clara, CA) running at 3.0 GHz with a total memory of 896 GB. The dose calculations were carried out using 20×10^6 photon histories in all cases. The computation times were on average 18 min for simulations over each phantom.

Dose calculations

The MC code simulates the photon interactions with the ICRP computational phantoms and the imparted energies from both primary and scattered components in each voxel can be calculated. This information was used to generate three-dimensional energy distributions and compute the total absorbed energy in groups of voxels making up each organ or tissue. The absorbed doses to an organ/tissue were calculated as the ratio between the total imparted energy to the voxels included in the organ and the total mass of the organ. Although not required for the effective dose calculation, the organ dose to the eye lens was also considered for all of the imaging protocols.

To estimate the skeleton absorbed doses, the way in which the information concerning RBM, YBM and endosteum contents are coded in ICRP Report 110 was tailored to our program.[16] To calculate the energy absorbed by the RBM and endosteum in each voxel with spongiosa, the corresponding mass–energy absorption coefficients,[20] weighted with the fractional mass of RBM, YRM and endosteum, were used.[21] Moreover, an enhancement factor was applied to the energy absorbed by the RBM to account for the effect of secondary electrons produced in cortical bone, which considered six categories according to the trabecular or RBM content of the bone represented in each voxel.[22] The absorbed dose in RBM/endosteum was then obtained as the quotient between the energy absorbed in RBM/endosteum and the total mass of RBM/endosteum in each phantom. In a previous work, to validate our MC program, the relative uncertainties associated with dose calculations, including random and non-random components, were estimated to be in the range 4–5%.[15] The same approach was used to assess uncertainties related to organ dose calculation in this work.

From the organ/tissue dose results for each phantom, the sex-averaged effective dose (E) was computed for all the simulated protocols according to ICRP Report 103 using the following equation:[7]

$$E = \sum w_T \frac{H_T^M + H_T^F}{2} \quad (1)$$

Where w_T is the weighting factor for tissue T, and H_T^M and H_T^F are the equivalent doses in the organ or tissue T of AM and AF phantoms, respectively. In our study, these values are numerically equal to those of the absorbed dose in the organ/tissue because the radiation weighting factor (w_R) for X-rays has the value of 1. The remainder tissues of AM and AF phantoms were included in the calculation. Additionally, sex-averaged normalized effective dose values to the tube loading settings (computed as E per mAs) were also obtained for each protocol.

Dose measurements

The dose–area product (DAP) was measured for each of the analysed protocols. DAP values are displayed in the console of several current CBCT devices, and this quantity has the potential to be used as a broad estimate of effective dose using suitable conversion factors.[23] DAP was measured using a transmission chamber type 70157 connected to a Doseguard 100 model electrometer (RTI Electronics, Mölndal, Sweden), which was placed at the X-ray exit window and calibrated with a beam quality that was equivalent to that of the CBCT device. The statistical variation in the sets of DAP measurements was combined with other components, coming from different sources, to assess an upper bound for the uncertainties in the reported values.

For each protocol, a DAP to effective dose conversion factor (E/DAP) was derived as the quotient between the simulated E values and measured DAP values. The term E_{DAP} was utilized as a parameter because of its similarity to E_{DLP} for converting dose–length product values into E for CT use.

Results

The maximum percentage difference between the calculated and the tabulated ICRP organ and tissue masses was 1% corresponding to the eye lens. These differences can be considered as negligible because they were observed for small organs and related to computation rounding effects.

Table 2 shows DAP values and the calculated sex-averaged effective dose values E for the different scan protocols, including full and half rotation. The E_{DAP} and E values, normalized to the selected tube loading settings, are also displayed. The relative uncertainties associated with the reported DAP values were estimated to be in the range 8–10%, and they were mainly due to DAP–meter calibration, differences in beam quality and FOV size.

The organ dose values varied between the selected scan volumes and substantially differed between the AM and AF phantoms (Tables 3 and 4). Higher values were obtained for the AF phantom in all organs/tissues excluding the brain. Similar trends were found for both rotation modes: organ doses for 180° were approximately 40% lower (25–58% range) than those calculated for 360° acquisitions (Figure 2). The relative ;uncertainties associated with organ doses were as large as 4%. The main contribution to them was due to sources that are essentially organ independent, such as X-ray spectrum and radiation beam geometry, including total filtration and field size.

Regarding the average contribution of each organ to the effective dose ($w_T \times H_T/E$), the highest value (31%; 27–36% range) corresponded to the remainder, followed by the salivary glands (23%; 20–29% range), thyroid (13%; 8–17% range), RBM (10%; 9–11% range) and oesophagus (7%; 4–10% range).

The values of organ dose to the eye lens and thyroid for different FOV positions in the AF phantom are represented in the graphs in Figure 3. A dramatic increase in dose can be observed in both cases, being more significant in the thyroid (0.2–1.6 mGy) than in the eye lens (0.2–0.9 mGy). The other organs/tissues situated at the edge of the radiation field showing positiondependent dose values were the oesophagus (which might receive doses up to sixfold higher depending on the fraction included in the direct beam) and the brain.

Discussion

An MC-based method was used to estimate organ doses in reference computational phantoms of both sexes by taking the actual CBCT device exposure parameters as inputs. The calculated organ doses in both phantoms have been used: first, to identify for each examination the organs with the highest risk and, second, to estimate sex-averaged values of E.

As expected, E values showed a strong primary dependence on the field size (from 25 μSv for the smallest FOV and up to 66 μSv for the largest FOV in landscape mode) because as the FOV decreased there were organs/tissues either entirely or partially excluded from the direct beam, and also the scattered radiation decreased. Our findings are within the range of recently published values for the same CBCT device and are slightly lower than those published by other authors, excluding the full-head scan, for which a significantly lower sex-averaged E value (46 μSv) was found.[2,8,10–13,15] This is a special acquisition, with the detector rotated into a portrait mode and the centre of rotation offset to capture a larger FOV, in which some of the organs (salivary glands, lymphatic nodes) are exposed during only part of the acquisition. In Figure 4, the FOV and the dose maps for the Ø16 × 13 cm height and the full-head (Ø23 × 17 cm height) protocols are depicted for the AF phantom. The borders of both FOVs are clearly differentiated in the respective coronal and sagittal images. In particular, the asymmetry of the dose distribution for the full-head FOV is noticeable, especially in the axial section.

The value of E for the 6 cm mandible scan was somewhat higher than the value corresponding to the 6 cm maxilla scan. Such values were close to those measured within an adolescent hermaphrodite phantom.[24] Similar values for the maxilla and markedly higher values for the mandible in adult patients have been reported by different authors.[10,11] By contrast, E values obtained by Loubele et al[1] from TLD measurements within phantoms were higher for the acquisition of maxilla.

Table 2 Dose–area product (mGy cm^2), sex-averaged effective dose E (μSv), E_{DAP} mSv mGy^{-1} cm^{-2} and normalized E (μSv mAs^{-1}) for 360° and 180° acquisitions

	Full rotation				*Half rotation*			
Protocol	*DAP*	*E*	E_{DAP}	*E/mAs*	*DAP*	*E*	E_{DAP}	*E/mAs*
Ø16 × 13 cm height	556	66	0.12	3.6	303	40	0.13	4.0
Ø16 × 11 cm height	476	58	0.12	3.2	260	36	0.14	3.6
Ø16 × 10 cm height	415	53	0.13	2.8	226	32	0.14	3.2
Ø16 × 8 cm height	361	47	0.13	2.5	197	29	0.15	2.8
Ø16 × 6 cm height, maxilla	276	35	0.13	1.9	151	22	0.14	2.1
Ø16 × 6 cm height, mandible	270	39	0.14	2.1	147	24	0.16	2.3
Ø16 × 4 cm height	181	25	0.14	1.4	98	16	0.16	1.5
Ø8 × 8 cm height	214	29	0.14	1.6	117	18	0.16	1.8
Ø23 × 17 cm height, full head	443	46	0.10	2.5	241	24	0.10	2.4

Table 3 Dose to organs for adult male (AM) and adult female (AF) phantoms for large field of view 360° acquisitions

	Scan volume			
	Ø16 × 13 cm	*Ø16 × 11 cm*	*Ø16 × 10 cm*	*Ø23 × 17 cm full head*
	Dose (mGy)			
Organ/tissue	*AM/AF*	*AM/AF*	*AM/AF*	*AM/AF*
Red bone marrow	0.05/0.07	0.04/0.05	0.03/0.05	0.04/0.05
Oesophagus	0.04/0.18	0.04/0.18	0.04/0.18	0.02/0.10
Thyroid	0.08/0.30	0.08/0.29	0.07/0.28	0.05/0.18
Skin	0.08/0.08	0.06/0.07	0.05/0.06	0.06/0.07
Bone surface	0.20/0.42	0.15/0.29	0.12/0.22	0.16/0.36
Brain	0.59/0.38	0.31/0.16	0.19/0.09	0.66/0.52
Salivary glands	1.27/1.67	1.23/1.59	1.15/1.39	0.85/1.05
Lymphatic nodes	0.07/0.12	0.07/0.11	0.07/0.11	0.04/0.08
Oral mucosa	0.76/1.12	0.72/1.08	0.70/1.04	0.54/0.77
Extrathoracic region	0.70/1.21	0.57/1.11	0.43/0.96	0.50/0.79
Eye lens	0.44/0.87	0.13/0.14	0.08/0.09	0.66/0.61

Such discrepancies might be explained by different modelling of the salivary glands and RBM and by differences in size and positioning of the thyroid within the computational or physical phantoms used.

The values of E for the 180° acquisitions were systematically greater than the corresponding halved E values for full rotation and the same FOV (differences in the range 38–48%). This effect has two main causes: first, the exposure angle for a half rotation is approximately 55% of that for full rotation and, second, the proportion in which several tissues/organs are exposed is different for each mode, because the X-ray tube rotates behind the patient's head during 180° acquisition. The calculated effective doses for high-resolution acquisitions, with twice the number of radiation pulses, and thus double tube loading settings, gave dose values twofold the corresponding doses for a standard resolution acquisition, as predicted.

As stated by the ICRP, E should not be used for epidemiological studies. Moreover, for retrospective dose and risk assessments in individual cases, parameters such as sex, age and organ doses would require consideration.[7] Therefore, it can be useful to analyse the differences in the organ doses obtained separately for the male and female models. It was found that the contribution to the effective dose of each phantom was uneven because organ/tissue doses in the phantom AF were higher than the corresponding doses in the AM phantom for the vast majority of the organs. Excluding breast, for which the dose in AF was on average four times higher than in AM, but with a negligible impact to E, the most relevant differences in dose between the AF and AM phantoms were found for the thyroid, bone surface, extrathoracic region, oral mucosa and lungs (Tables 3 and 4). In contrast, although the relative differences between the phantoms are lower, the dose values to other organs/tissues, such as lymphatic nodes or eye lenses, show strong variations depending upon the field size used.

The relative difference in body mass between the AF and AM phantoms (19%, Table 1) is 42% on average when including only the organs that contribute most to the effective dose. Additionally, the differences in body and organ shape and organ location between both computational models cause more AF phantom organs (or larger portions of them) to be inside the primary beam, whereas for the AM phantom, they are completely or partially in the low-dose scatter region (Figure 1). This effect clearly occurs for several organs/tissues, such as the oesophagus, thyroid, bone surface, extrathoracic region and, to some extent, eye lenses. When comparing our

Table 4 Dose to organs for adult male (AM) and adult female (AF) phantoms for small and medium field of view 360° acquisitions

	Scan volume				
	Ø16 × 8 cm	*Ø16 × 6 cm maxilla*	*Ø16 × 6 cm mandible*	*Ø16 × 4 cm*	*Ø8 × 8 cm*
	Dose (mGy)				
Organ/tissue	*AM/AF*	*AM/AF*	*AM/AF*	*AM/AF*	*AM/AF*
Red bone marrow	0.03/0.04	0.02/0.03	0.03/0.04	0.02/0.02	0.02/0.03
Oesophagus	0.03/0.17	0.02/0.05	0.03/0.17	0.01/0.05	0.02/0.13
Thyroid	0.07/0.28	0.03/0.11	0.06/0.26	0.03/0.11	0.05/0.19
Skin	0.04/0.05	0.04/0.04	0.03/0.04	0.02/0.03	0.03/0.04
Bone surface	0.10/0.18	0.09/0.16	0.07/0.14	0.05/0.10	0.06/0.13
Brain	0.12/0.06	0.16/0.08	0.07/0.04	0.06/0.03	0.09/0.05
Salivary glands	1.07/1.11	0.87/1.19	0.87/0.76	0.68/0.67	0.58/0.59
Lymphatic nodes	0.07/0.09	0.04/0.07	0.06/0.07	0.04/0.05	0.04/0.06
Oral mucosa	0.67/0.99	0.56/0.93	0.61/0.78	0.52/0.71	0.36/0.52
Extrathoracic region	0.32/0.79	0.32/0.72	0.22/0.60	0.15/0.45	0.17/0.44
Eye lens	0.06/0.05	0.07/0.07	0.04/0.03	0.03/0.03	0.04/0.03

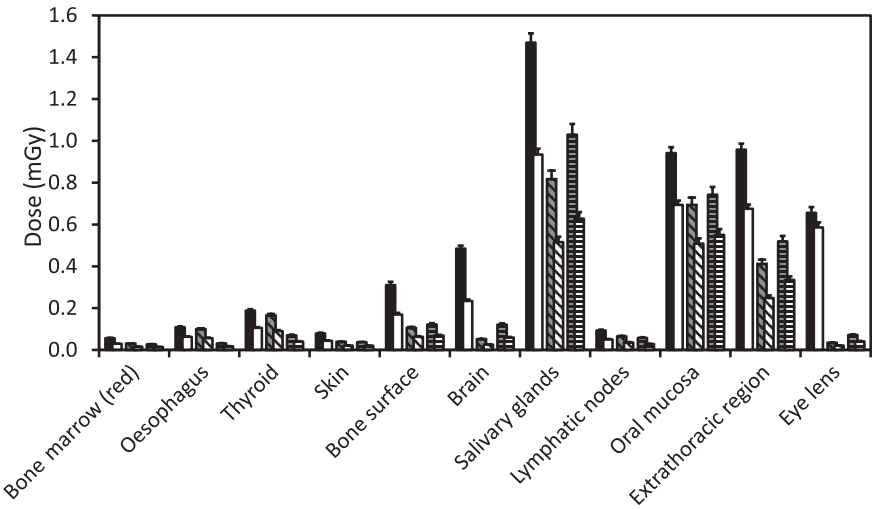

Figure 2 Sex-averaged dose to organs for full- and half-rotation protocols. ■, 16 × 13 cm full rotation; □, 16 × 13 cm half rotation; ▨, 16 × 6 cm mandible full rotation; ▨, 16 × 6 cm mandible half rotation; ▤, 16 × 6 cm maxilla full rotation; ▤, 16 × 6 cm maxilla half rotation

results with those from the literature, large differences were found for several organs/tissues, such as RBM and bone surface, which may stem from the inherent difficulty of measuring dose in these tissues.[14] For other organs (*i.e.* salivary glands, brain, thyroid and extrathoracic region), our dose values for the AF phantom were close to those measured by other authors.[2,14] This fact, which can be explained by a better anatomical correspondence between our female model and the phantoms utilized for the experimental measurements, highlights the need for age and sex-specific models to accurately assess the risk associated with diagnostic exposures.

The analysis of the influence of FOV shifting along the *z*-axis showed differences of six- to eightfold in the dose delivered to the eye lens or thyroid (Figure 3). In the case of eye lenses, a large difference in dose can be occasioned by FOV shifts of only 1.5 cm, whereas the dose increase in the thyroid required a large shift (6cm) due to its larger size and ease for remaining outside of the field. The dose to the eye lens is well below the deterministic dose thresholds and there is no cancer risk involved, and only a large number of scans could potentially result in a deterministic effect. Not-withstanding this, to avoid the deleterious effects of radiation, several authors proposed the use of leaded glasses to reduce the radiation dose to the eye lens, especially in paediatric patients.[25] For the thyroid, the cancer risk increases with dose, and even small doses have the potential of causing radiation-induced cancer. For all these reasons, as recommended, when using imaging X-rays, it is essential for patient protection to fit the radiation field to the minimum size compatible with the clinical task. This paradigm applies in general and for CBCT examinations.[5]

With the results obtained for the effective dose and DAP for all protocols (excluding the full head), a linear fit to obtain the best estimate of E_{DAP} was performed.

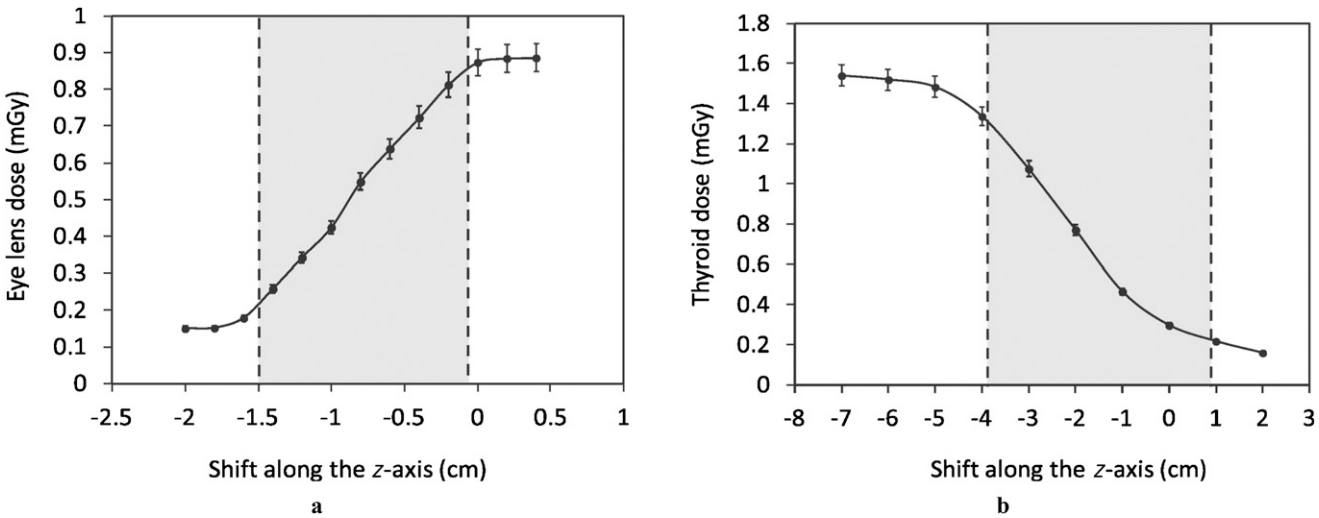

Figure 3 Eye lens (a) and thyroid dose (b) when shifting the field of view along the cone beam CT rotational axis. The original position of the field border corresponds to a "0" displacement. The positive and negative values correspond to upward and downward shifts. The grey area represents the coverage of each organ along the axis. The lines between the points are connectors without meaning

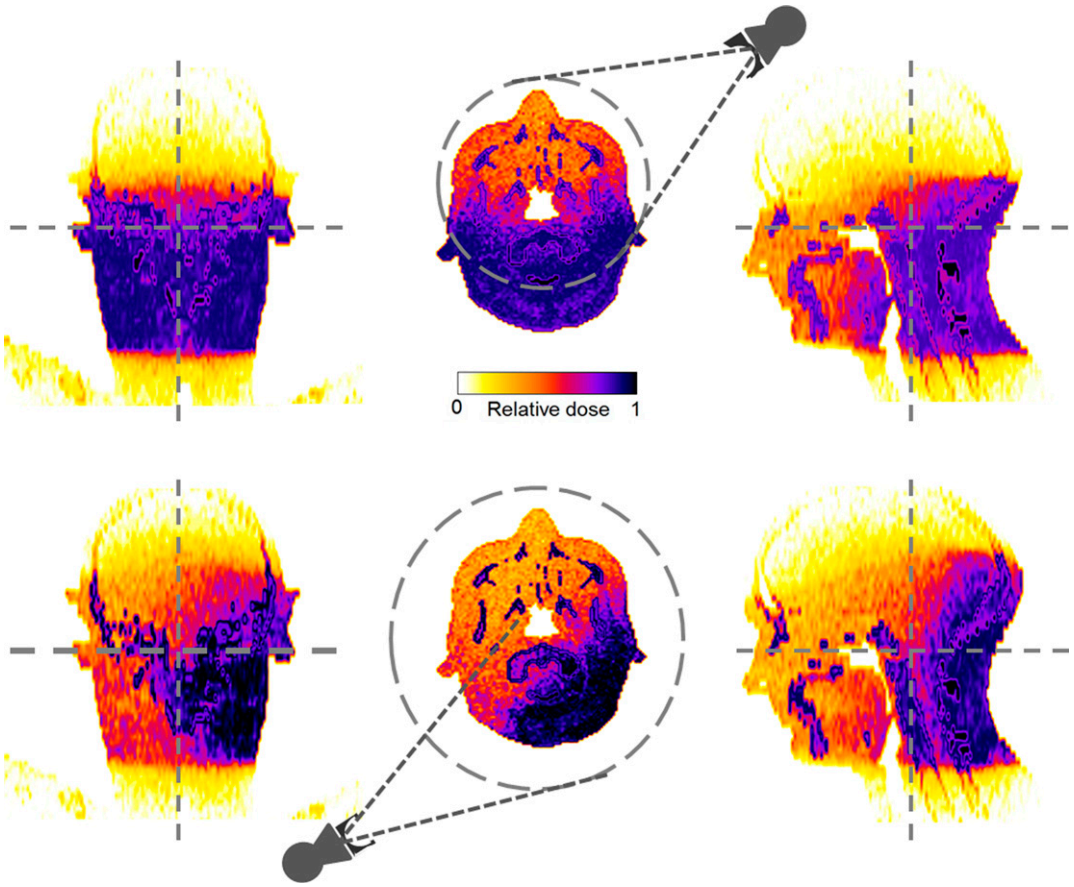

Figure 4 Field of view and dose maps for the Ø16 × 13 cm height (top) and the full-head (Ø23 × 17 cm height) (bottom) protocols for coronal, axial and sagittal sections of the International Commission on Radiological Protection adult female (AF) phantom

The full-head protocol was excluded because of its different geometry compared with landscape protocols that produces an uneven exposure in several relevant organs, such as salivary glands or lymphatic nodes. The linear regression, with zero intercept, over the whole sample of 180° and 360° acquisitions, shown in Figure 5, yielded a slope of 0.130 ($R^2 = 0.994$; 95% confidence interval 0.124–0.135). Given that the uncertainties associated with the reported values of E and DAP can be as large as 10% each,[26,27] it is considered that this E_{DAP} value 0.130 ± 0.006 μSv mGy^{-1} cm^{-2}) can be useful, to an acceptable extent, for making broad estimations of the effective dose from the DAP values obtained from either direct measurement or the equipment console display.

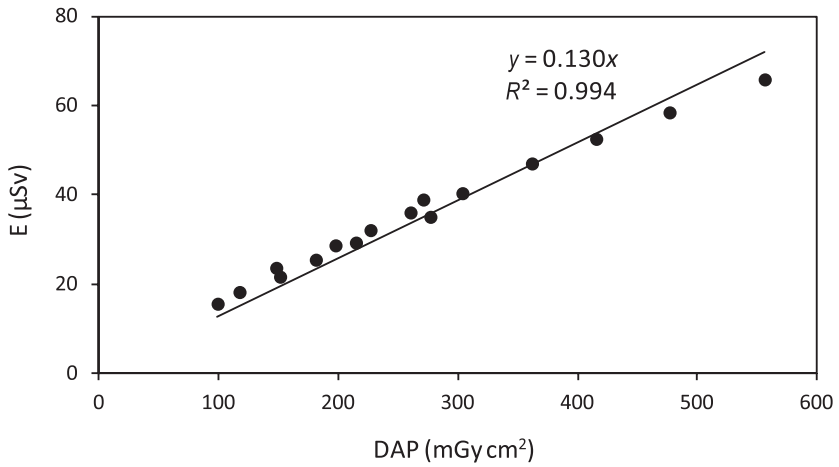

Figure 5 Effective dose (μSv) and dose–area product (mGy cm^2) for both full and half rotation and all of the investigated fields of view, excluding the full head, together with the linear fit

The effective dose is a quantity that should be managed with caution but can be useful for comparing the average risk from examinations in the same or similar CBCT devices. The derivation of similar values of E_{DAP} for other CBCT devices is expected in the near future.

In conclusion, the MC method was applied to calculate organ doses and effective dose from CBCT imaging in dental and maxillofacial radiology using realistic male and female anthropomorphic computational phantoms for a wide range of protocols of a specific device. From these results, differences in the organ doses between protocols and phantom sex were discussed. Further, the potential for performing a comparison between protocols and CBCT manufacturers and models was realized. When analysing dose variation in peripheral organs, dramatic increases in both eye lens and thyroid doses were obtained with FOV shifting. A single DAP to effective dose conversion factor can be used to assess effective doses for landscape acquisitions. The applied methodology is considered sufficiently accurate to be used in other dental CBCT equipment.

Acknowledgments

This research has been partly performed using the CESCA (Centre de Supercomputació de Catalunya) resources.

References

1. Loubele M, Bogaerts R, Van Dijck E, Pauwels R, Vanheusden S, Suetens P, et al. Comparison between effective radiation dose of CBCT and MSCT scanners for dentomaxillofacial applications. *Eur J Radiol* 2009; **71**: 461–468.
2. Ludlow JB, Ivanovic M. Comparative dosimetry of dental CBCT devices and 64-slice CT for oral and maxillofacial radiology. *Oral Surg Oral Med Oral Pathol Oral Radiol Endod* 2008; **106**: 106–114.
3. Guerrero ME, Jacobs R, Loubele M, Schutyser F, Suetens P, van Steenberghe D. State-of-the-art on cone beam CT imaging for preoperative planning of implant placement. *Clin Oral Investig* 2006; **10**: 1–7.
4. De Vos W, Casselman J, Swennen GR. Cone-beam computerized tomography (CBCT) imaging of the oral and maxillofacial region: a systemic review of the literature. *Int J Oral Maxillofac Surg* 2009; **38**: 609–625.
5. SEDENTEXTCT. Radiation protection: cone beam CT for dental and maxillofacial radiology. Evidence based guidelines 2011. Available from http://www.sedentexct.eu/files/guidelines_final.pdf.
6. International Commission on Radiological Protection. *1990 Recommendations of the International Commission on Radiological Protection*. ICRP Publication 60. Ann ICRP 21. Oxford, UK: Pergamon Press; 1991.
7. International Commission on Radiological Protection. *2008 Recommendations of the International Commission on Radiological Protection*. ICRP Publication 103. Ann ICRP 37. Amsterdam: Elsevier; 2007.
8. Ludlow JB, Davies-Ludlow LE, White SC. Patient risk related to common dental radiographic examinations: the impact of 2007 International Commission on Radiological Protection recommendations regarding dose calculation. *J Am Dent Assoc* 2008; **139**: 1237–1243.
9. Qu XM, Li G, Ludlow JB, Zhang ZY, Ma XC. Effective radiation dose of ProMax 3D cone-beam computerized tomography scanner with different dental protocols. *Oral Surg Oral Med Oral Pathol Oral Radiol Endod* 2010; **110**: 770–776.
10. Roberts JA, Drage NA, Davies J, Thomas DW. Effective dose from cone beam CT examinations in dentistry. *Br J Radiol* 2009; **82**: 35–40.
11. Davies J, Johnson B, Drage NA. Effective doses from cone beam CT investigation of the jaws. *Dentomaxillofac Radiol* 2012; **41**: 30–36.
12. Silva MA, Wolf U, Heinicke F, Bumann A, Visser H, Hirsch E. Cone-beam computed tomography for routine orthodontic treatment planning: a radiation dose evaluation. *Am J Orthod Dentofacial Orthop* 2008; **133**: 640.e1–5.
13. Ludlow JB, Davies-Ludlow LE, Brooks SL, Howerton WB. Dosimetry of 3 CBCT devices for oral and maxillofacial radiology: CB Mercuray, NewTom 3G and i-CAT. *Dentomaxillofac Radiol* 2006; **35**: 219–226.
14. Pauwels R, Beinsberger J, Collaert B, Theodorakou C, Rogers J, Walker A, et al. Effective dose range for dental cone beam computed tomography scanners. *Eur J Radiol* 2012; **81**: 267–271.
15. Morant JJ, Salvad M, Casanovas R, Hernandez-Giron I, Velasco E, Calzado A. Validation of a Monte Carlo simulation for dose assessment in dental cone beam CT examinations. *Phys Med* 2012; **28**: 200–209.
16. International Commission on Radiological Protection. *Adult reference computational phantoms*. ICRP Publication 110. Ann ICRP 39. Amsterdam, Netherlands: Elsevier; 2009.
17. Zhang G, Pauwels R, Marshall N, Shaheen E, Nuyts J, Jacobs R, et al. Development and validation of a hybrid simulation technique for cone beam CT: application to an oral imaging system. *Phys Med Biol* 2011; **56**: 5823–5843.
18. Nelson WR, Hirayama H, Rogers DWO. *The EGS code system*. Technical Report SLAC-265. Menlo Park, CA: Stanford Linear Accelerator Center; 1985.
19. Hirayama H, Namito Y, Ban S. Implementation of a general treatment of photoelectric-related phenomena for compounds or mixtures in EGS4. KEK Internal Report 2000-3, May 2000 [accessed April 2010]. Available from: http://ccwww.kek.jp/kek/rad/egs4/photo.pdf
20. Hubbell JH, Seltzer SM. Tables of X-ray mass attenuation coefficients and mass energy-absorption coefficients. 1996; U.S. Secretary of Commerce on behalf of the United States of America. Available from http://physics.nist.gov/PhysRef/Data/X-rayMassCoef/cover.html.
21. Lee C, Lee C, Shah AP, Bolch WE. An assessment of bone marrow and bone endosteum dosimetry methods for photon sources. *Phys Med Biol* 2006; **51**: 5391–5407.
22. King SD, Spiers FW. Photoelectron enhancement of the absorbed dose from X rays to human bone marrow: experimental and theoretical studies. *Br J Radiol* 1985; **58**: 345–356.
23. Lofthag-Hansen S, Thilander-Klang A, Ekestubbe A, Helmrot E, Grndahl K. Calculating effective dose on a cone beam computed tomography device: 3D Accuitomo and 3D Accuitomo FPD. *Dentomaxillofac Radiol* 2008; **37**: 72–79.
24. Theodorakou C, Walker A, Horner K, Pauwels R, Bogaerts R, Jacobs R, et al. Estimation of paediatric organ and effective doses from dental cone beam CT using anthropomorphic phantoms. *Br J Radiol* 2012; **85**: 153–160.
25. Prins R, Dauer LT, Colosi DC, Quinn B, Kleiman NJ, Bohle GC, et al. Significant reduction in dental cone beam computed tomography (CBCT) eye dose through the use of leaded glasses. *Oral Surg Oral Med Oral Pathol Oral Radiol Endod* 2011; **112**: 502–507.
26. Martin CJ. Effective dose: how should it be applied to medical exposures? *Br J Radiol* 2007; **80**: 639–647.
27. Larsson PL. Calibration of ionization chambers for measuring air kerma integrated over beam area in diagnostic radiology. Thesis, Linköping University, 2006.